Thin Lamina Cribrosa Beams Have Different Collagen Microstructure Than Thick Beams

Bryn L. Brazile,[1] Yi Hua,[1] Ning-Jiun Jan,[1,2] Jacob Wallace,[1] Alexandra Gogola,[1] and Ian A. Sigal[1–4]

[1]Department of Ophthalmology, University of Pittsburgh School of Medicine, Pittsburgh, Pennsylvania, United States
[2]Department of Bioengineering, Swanson School of Engineering, University of Pittsburgh, Pittsburgh, Pennsylvania, United States
[3]McGowan Institute for Regenerative Medicine, University of Pittsburgh School of Medicine and University of Pittsburgh, Pittsburgh, Pennsylvania, United States
[4]The Louis J. Fox Center for Vision Restoration of UPMC and the University of Pittsburgh, Pittsburgh, Pennsylvania, United States

PURPOSE. To compare the collagen microstructural crimp characteristics between thin and thick lamina cribrosa (LC) beams.

METHODS. Seven eyes from four sheep were fixed at 5 mm Hg IOP in 10% formalin. For each eye, one to three coronal cryosections through the LC were imaged with polarized light microscopy and analyzed to visualize the LC and determine collagen fiber microstructure. For every beam, we measured its width and three characteristics of the crimp of its collagen fibers: waviness, tortuosity, and amplitude. Linear mixed effects models were used to test whether crimp characteristics were associated with the LC beam width.

RESULTS. For each eye and over all the eyes, LC beam width was positively associated with crimp waviness and tortuosity, and negatively associated with crimp amplitude (P's < 0.0001). Thin beams, average width 13.11 μm, had average (SD) waviness, tortuosity, and amplitude of 0.27 (0.17) radians, 1.017 (0.028) and 1.88 (1.41) μm, respectively. For thick beams, average width 26.10 μm, these characteristics were 0.33 (0.18) radians, 1.025 (0.037) and 1.58 (1.36) μm, respectively.

CONCLUSIONS. Our results suggest heterogeneity in LC beam mechanical properties. Thin beams were less wavy than their thicker counterparts, suggesting that thin beams may stiffen at lower IOP than thick beams. This difference may allow thin beams to support similar amounts of IOP-induced force as thicker beams, thus providing a similar level of structural support to the axons at physiologic IOP, despite the differences in width. Measurements of beam-level mechanical properties are needed to confirm these predictions.

Keywords: optic nerve head, collagen, crimp, lamina cribrosa, intraocular pressure, microstructure, biomechanics

The lamina cribrosa (LC) is a trabecular structure consisting of an intricate network of collagenous beams and blood vessels that support the delicate retinal ganglion cell (RGC) axons passing through the pores.[1] It is often considered that mechanical insult within the LC contributes to glaucomatous damage.[1–6] This may involve several paths, such as compression or shearing of the RGC axons potentially affecting axoplasmic transport,[3,7] stretch-induced activation of astrocytes,[8–13] or disruption of the vasculature and ischemia.[7,11,14,15] Overall, a larger mechanical insult is thought to translate into a higher likelihood of neural tissue damage.[16,17]

The wide variation in width of the collagenous beams of the LC has been proposed to be indicative of mechanical support that the beams provide to the surrounding tissues, both when interpreting images and in modeling.[5,18–21] In this view, thin beams are structurally weaker than thick beams, stretching more under a given IOP, a larger mechanical insult, potentially endangering nearby axons. There are, however, some problems with this view. First, it remains to be proven that RGC axon damage in LC regions with thin beams is more pronounced or occurs earlier in the disease than in regions with thick beams.

Second, the structural stiffness of a beam is not only determined by its width, but also by its mechanical properties. The mechanical properties of a beam are, in turn, determined by its composition and organization at the microstructural level. At this level, the collagen fibers exhibit natural undulations called crimp (Fig. 1). As is well-known from other collagenous soft-tissues,[22–25] this crimp is central to the nonlinear stiffening behavior of the beams, and how much they deform under the loads of IOP (Fig. 2).

If thin and thick LC beams have different collagen microstructural crimp characteristics, it would indicate that they also have different mechanical properties, and therefore that beam width is not sufficient to infer the structural stiffness of a beam or the support it provides to adjacent tissues. Our goal in this project was to measure the collagen fiber crimp characteristics of LC beams and determine whether beam width is associated with three measures of collagen crimp: waviness, tortuosity, and amplitude. For this, we used techniques based on polarized light microscopy (PLM) that we have recently demonstrated as suitable for direct measurement of collagen crimp in ocular tissues.[26–31]

Investigative Ophthalmology & Visual Science
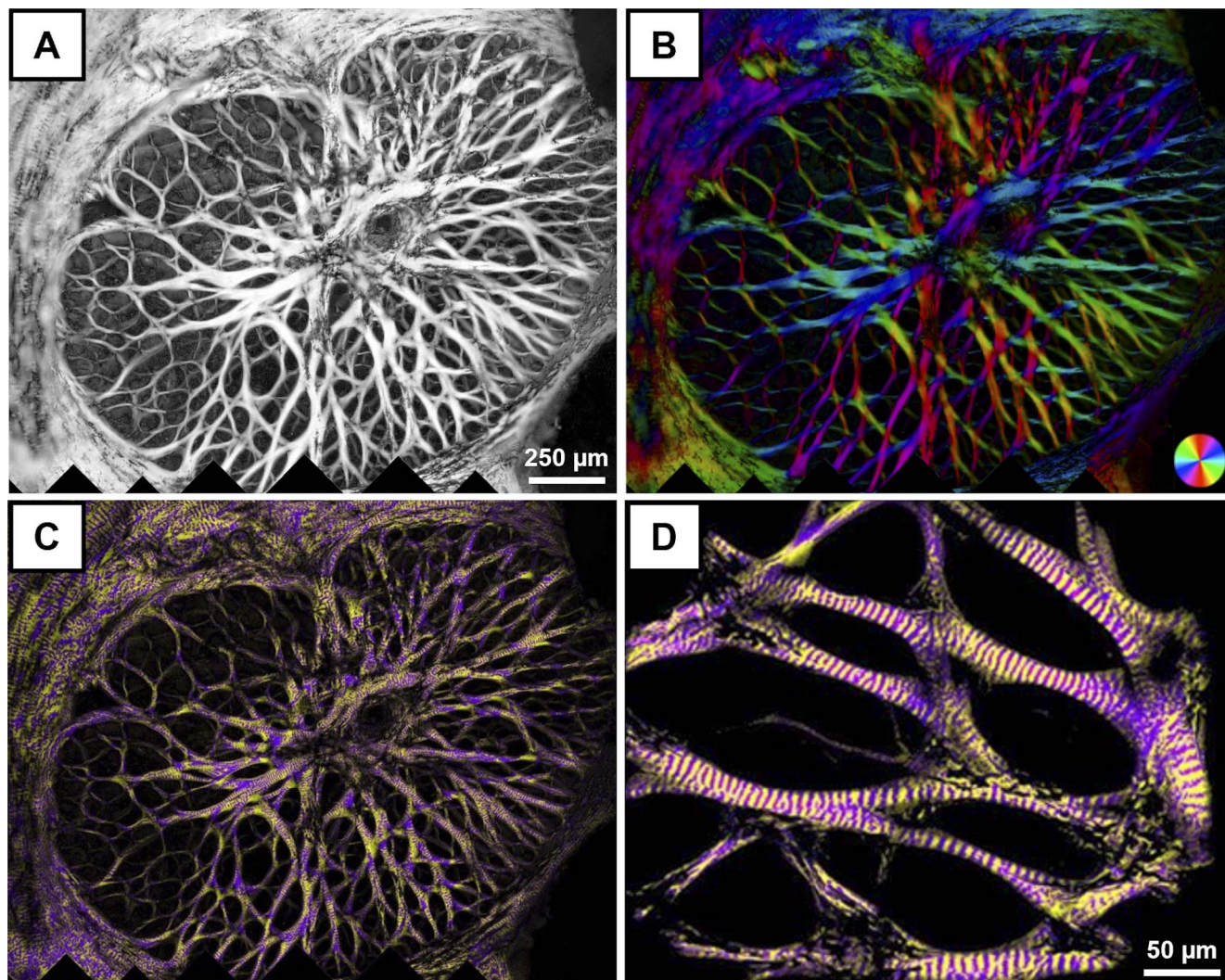
FIGURE 1. Visualization of the LC of a sheep eye fixed at 5 mm Hg. Coronal sections through the LC were imaged with PLM, and processed as described elsewhere[27,28] to obtain an "energy" parameter (**A**), local fiber orientation (**B**), and visualize crimp (**C, D**). In the orientation map shown in (**B**), *colors* indicate local collagen fiber orientations, whereas intensity is scaled based on the energy shown in (**A**). The orientations were further processed to simplify visualizing collagen fiber undulations, or crimp, as described elsewhere.[27,28] The regular patterns of crimp in the LC beams are more clearly discernible as *yellow/purple bands* in LC close-ups (**D**).

METHODS

Sample Preparation

Seven eyes from four adult sheep, approximately 2 years old, were acquired from a local abattoir and processed within 8 hours of death following the procedure described elsewhere.[26-28,30,31] Briefly, the eyes were carefully cleaned to remove the muscles, fat, and episcleral tissues. Each eye was then cannulated through the anterior chamber with a 23-gauge needle to set IOP to 5 mm Hg using a saline column. The eyes were then fixed with 10% formalin for 24 hours while maintaining IOP. Following fixation, the optic nerve head (ONH) within the posterior pole was excised using an 11.5-mm-diameter trephine and cryosectioned coronally into 30-μm-thick sections. One to three sections through the LC, per eye, were selected for analysis. Note that the process required no labels or stains, no embedding in paraffin or plastic, and no dehydration.

Imaging Acquisition

The sections were imaged using PLM following previously reported protocols (Fig. 1).[26-31] Briefly, two filters (Hoya, Tokyo, Japan) were used, one as a polarizer, and the other as an analyzer. Four images were acquired using white light illumination, with filter orientations rotated 45° between images. The relative changes in signal intensities at each pixel were used to compute local collagen fiber orientation using custom code in Fiji Is Just ImageJ.[32] To facilitate visualization, we also computed an "energy" parameter.[26-31] Briefly, this parameter measures the variations in pixel intensity with rotations of the polarized filter. If there is no birefringent material (e.g., zero collagen density), the energy will be zero. Presence of in-plane collagen fibers would result in higher energy.[33] An Olympus BX60 microscope (Olympus, Tokyo, Japan) was used with a SPOT camera (SPOT Imaging Solutions, Sterling Heights, MI, USA) and a ×10 objective (numerical aperture 0.3). The acquired images were 12-bit grayscale with a pixel size of 0.73 μm.
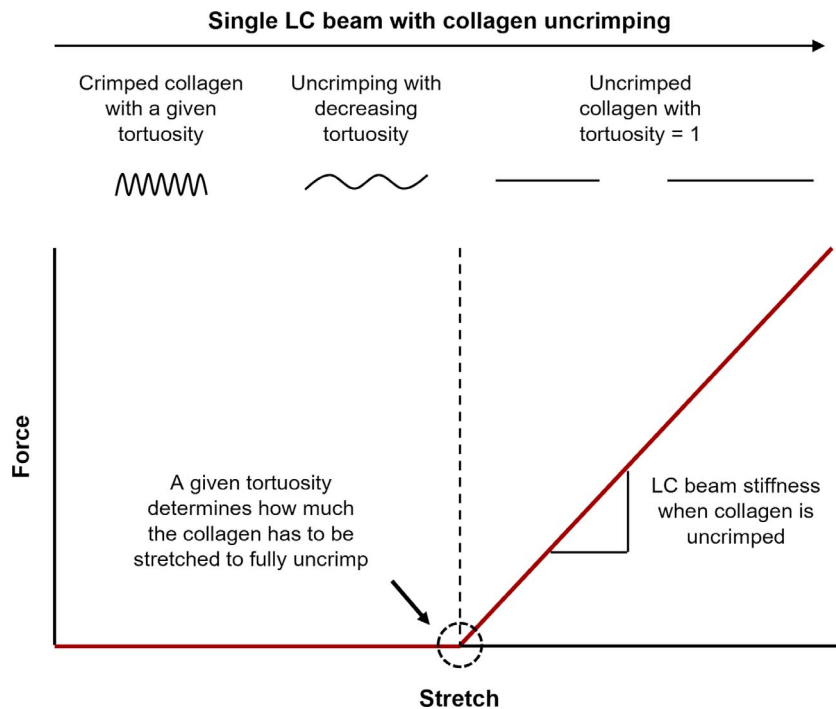
FIGURE 2. Schematic illustration of how the microstructural crimp determines the nonlinear stiffening behavior of a single LC beam. This diagram does not consider bending stiffness, and focuses solely on the longitudinal stretch of a collagen beam. As a beam stretches, its collagen uncrimps, requiring relatively little force until the collagen loses all crimp and is straight. The beam with straightened collagen can be stretched further only by making the fibers longer, which requires a larger, and increasing, force, and so the beam appears stiff.

LC Beam Width and Crimp Quantification

For every LC beam, we manually placed a straight-line segment across the middle of the beam to measure the beam width (red line, Fig. 3A). When marking, we were careful to make sure all LC beams in an image with an energy value greater than 2% of the energy range were marked and that the straight-line segment covered the entire width of the beam at the mid-point. We were also careful to not mark vessel walls or the thick tree-like stalk through the LC, sometimes called the ventral groove. From the manually placed width lines, a straight line through the center of the width line, perpendicular to it (longitudinal to the beam) was automatically generated, (green line, Fig. 3A). This line was then used to measure the waviness, tortuosity, and amplitude of the beam collagen. We verified that all longitudinal lines were fully within the beam and not on beam splits, divisions, overlaps, or other areas that could artifactually affect measurements (e.g., areas with very dense pigment). Note that the crimp of the collagen fibers in a beam may not be uniform. The crimp measurements in this work should be taken to represent the average crimp in the middle of a beam. In a preliminary study, we compared the crimp measures obtained with various longitudinal line lengths and found no significant differences in the calculated crimp parameters. Results with longitudinal lines 10 times as long as the beam width had less noise, and are therefore the ones shown in this article.

The crimp waviness, tortuosity, and amplitude were calculated using custom code as previously described (Fig. 3).[26,28,29,31] Briefly, crimp waviness was computed as the circular standard deviation of the orientation values (θ) of the pixels underlying the longitudinal line, in absolute values. Crimp tortuosity was computed as the ratio of the sum of the pixels' path length components to the sum of the end-to-end length components. Crimp amplitude was computed as the sum of the pixels' amplitude components. A beam with

perfectly straight fibers would have waviness and amplitude of zero, and tortuosity of 1. The parameters increase for beams with crimped fibers. It is important to note that the calculation of the crimp parameters was based on local fiber orientation values, which does not require direct visualization of the collagen fibers or discerning their edges. This is an important strength of PLM compared with other imaging techniques, which require clear visualization of fibers to determine orientation. We have discussed this in detail elsewhere.[26-31]

Statistical Analyses

Repeatability and Reproducibility of LC Beam Width and Crimp Measurements. Three markers manually placed line segments to measure the LC beam widths and to sample PLM-derived orientation information for crimp measurements. To ensure that these manually placed line segments produced repeatable and reproducible measurements, three markers measured the beam width and crimp parameters in 25 LC beams from different sections three times. For each of the 25 beams, the SDs of each marker's three measurements of beam width and crimp parameters were calculated. The largest SD across all 25 beams is reported here as the worst-case measure of repeatability. To calculate reproducibility, all measurements made from the three trials of three markers were pooled, and the SD was calculated for each beam. The largest SD of the pooled measurements was reported as the worst-case measure of reproducibility.

Crimp in Thin Versus Thick LC Beams. For simplicity, we first did an analysis splitting LC beams into "thin" and "thick" to test if thin beams have significantly different crimp parameters than thick beams. For each eye, beams that were less than or equal to the median beam width of that eye were labeled "thin" and those greater than the median were labeled "thick" (Supplementary Fig. S1). We calculated the medians, averages, and SDs of each crimp parameter for thin and thick
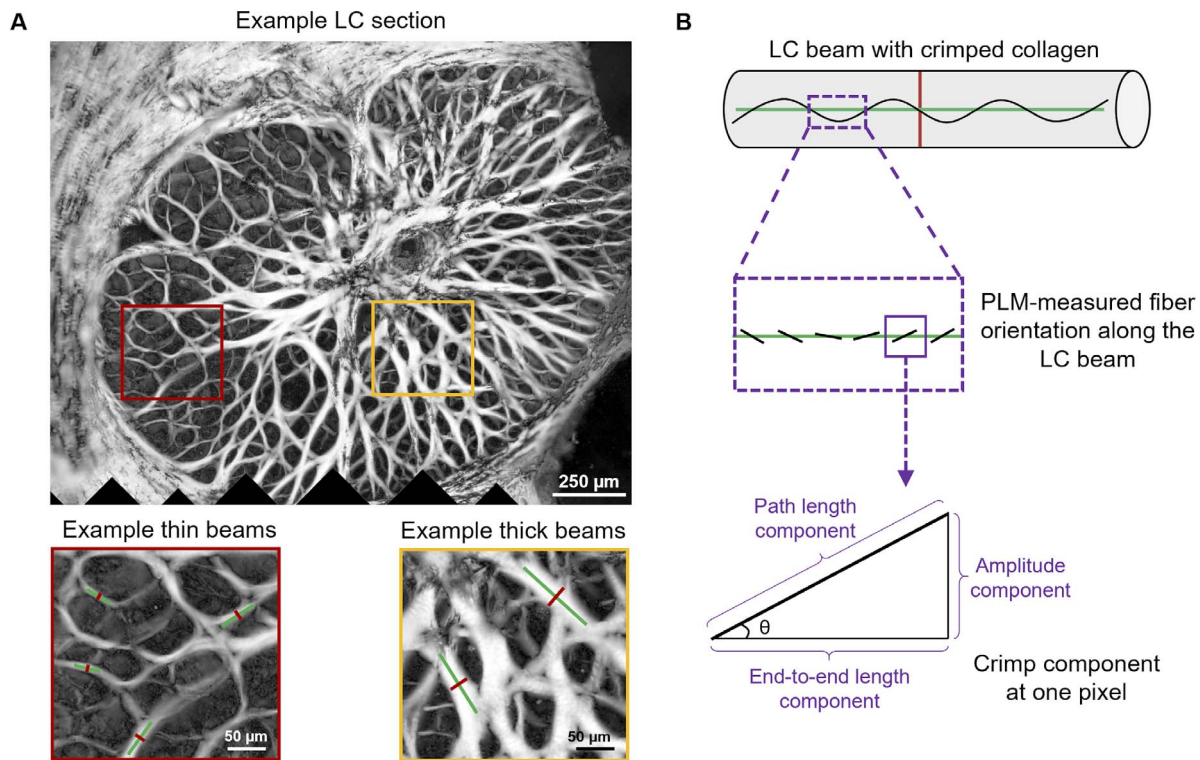
FIGURE 3. (**A**) Example LC section and close-ups to illustrate regions with thin and thick beams. On the beams are superimposed lines used to measure width (*red lines*) and crimp parameters (*green lines*). (**B**) Schematic of crimp parameter calculation. Trigonometric identities were used pixel by pixel along the line longitudinal to the beam (*green line*) to calculate the pixel level contributions to the amplitude, path length, and end-to-end length based on the local fiber orientation obtained from PLM. Pixel level contributions were integrated to compute total amplitude, path, and end-to-end lengths and determine crimp amplitude and tortuosity.

beams. Using linear mixed effects (LME) models, we determined whether crimp parameters of thin beams were significantly different from those of thick beams. LME models are linear models that incorporate fixed and random variables.[34] Fixed variables are our variables of interest, which in this case are whether a beam is thin or thick and the crimp parameters. Random variables are factors that may affect the sampling population, such as the number of measurements in different sections or in different eyes. LME models account for autocorrelation of measurements from the same section and eye.

Association of Crimp Parameters With LC Beam Width. We also used LME models to determine the relationship between each crimp parameter and LC beam width as a continuous variable. Specifically, we determined if each crimp parameter was associated with LC beam width within each individual eye, and whether they were associated with measurements pooled over all the seven eyes.

Plotting the measurements suggested that the relationship between the LC beam width and crimp parameters was not linear. Several models were therefore fit with crimp parameter transformations from the Box-Cox family (no transformation or linear, logarithmic, square, and square root). We used the Akaike information criterion (AIC) to select the optimal model among various transformations. AIC balances goodness of fit with the relative complexity of the model to avoid overfitting.

For all statistical tests, we used $\alpha = 0.01$ to establish significance. Note that significance is determined by the *P* value of the model, which is different from the AIC value. For example, it is possible that a model has a high AIC value but still shows significance with a low *P* value. All statistical analyses were done using R (v2.12.0).[34,35]

RESULTS

The LC beam width and crimp measurements were highly repeatable and reproducible. The LC beam width measurements had a repeatability of 1.7 μm and reproducibility of 2.8 μm. The repeatability of the measurements of crimp waviness, tortuosity, and amplitude were 0.036 radians, 0.0057 and 0.26 μm, respectively. The reproducibility of the measurements of crimp parameters were 0.069 radians, 0.0097 and 0.47 μm, respectively.

When splitting measurements by width into thin versus thick beams, we found that thin LC beams had significantly larger crimp waviness and tortuosity and smaller crimp amplitude than thick LC beams (*P*'s < 0.001), across all eyes as well as within each eye. Crimp distributions in thin and thick LC beams are shown in Figure 4. Average (SD) beam widths were 13.11 (4.71) μm for thin beams and 26.10 (10.28) μm for thick beams.

When treating LC beam width as a continuous variable, we found similar results. LC beam width was positively associated with the crimp waviness and tortuosity, and negatively associated with the crimp amplitude (*P*'s < 0.0001). We found this to be true for each eye (Supplementary Figs. S2–S4), as well as across all eyes (Fig. 5). After testing four model transformations (linear, square, and square root of the crimp parameter), we found that the optimal models (lowest AIC values) had beam width increasing with the square of the waviness and the square root of the tortuosity, and decreasing with the square root of the amplitude (Table; Supplementary Tables S1–S3).
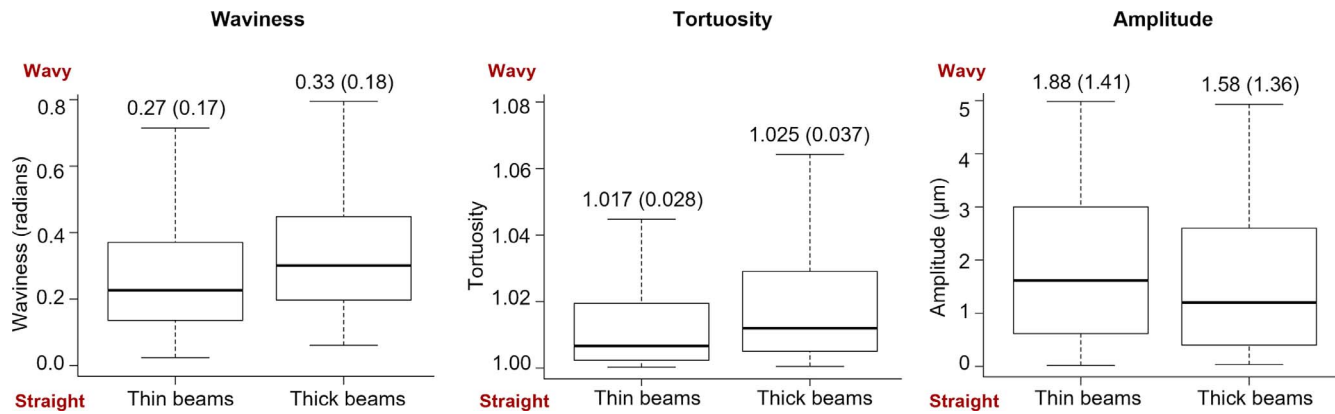
FIGURE 4. Boxplots of crimp distributions in thin and thick LC beams. Average (SD) beam widths were 13.11 (4.71) μm for thin beams and 26.10 (10.28) μm for thick beams. Average (SD) crimp waviness, tortuosity, and amplitude for thin and thick beams were labeled above the whisker's tip. Thick beams had significantly larger crimp waviness and tortuosity, and smaller crimp amplitude (P's < 0.001).

DISCUSSION

We found that LC beam collagen fiber crimp was significantly different between thin and thick beams. Specifically, waviness and tortuosity were positively associated with LC beam width, whereas crimp amplitude was negatively associated with LC beam width. Microstructural crimp is a major determinant of how collagenous tissues stiffen under stretch or tensile load,[25,26,36,37] and therefore our results imply that thin and thick beams require different amounts of stretch or force for their collagen fibers to straighten, and thus to stiffen. Thus, thin and thick LC beams should not be assumed to have the same mechanical properties. This is important, as it is evidence against the traditional assumption that LC beams have the same mechanical properties. Within this traditional assumption, the structural stiffness of an LC beam has been taken to be dependent only on its width. This perspective seemed reasonable, as it is essentially valid for trabecular bone, which looks similar to the LC.[38,39] Nevertheless, our results show that this is not the case in the LC, and therefore that it is likely not appropriate to estimate LC beam structural stiffness based only on its width.

To illustrate the potential implications of our findings, it is useful to consider two cases with different combinations of LC beam width and tortuosity: the traditional one and the one revised according to the findings presented herein (Fig. 6). The comparison is most clear when both thin and thick beams are considered under the same stretch conditions, and therefore this is the situation we illustrate. Nevertheless, it is possible that LC thin and thick beams in vivo are subjected to different stretch or loading conditions. However, we posit that ours is a useful comparison to understand the potential implications of our findings. Also, the same argument about differences in load or stretch could be made when attributing LC beam mechanical support based only on their width.

Interestingly, we found that the optimal model associated LC beam width with the square root of tortuosity. Rearranging the terms, this means that the optimal model was for a relationship between the square of the LC beam width and tortuosity. This suggests a mechanistic relationship between the cross-sectional LC beam area (proportional to the square of its diameter) and tortuosity. Such a relationship will help compensate the increase in stress due to the smaller cross-sectional area in thin beams, resulting in a more homogeneous force on the loaded collagen fibers. In this regard, it seems reasonable to hypothesize that the heterogeneity in collagen crimp may compensate for the heterogeneity in beam width, and vice versa.

The heterogeneity in beam crimp and width suggests that the LC may have a more gradual stiffening response to stretch than if it had a single beam crimp and width. This may help avoid sharp increases and reduce spatial inhomogeneities in LC deformation that could have advantages for the cells resident in the LC and the axons within.

It is important to acknowledge that, although crimp plays a central role on soft tissue mechanics, it is not the only factor
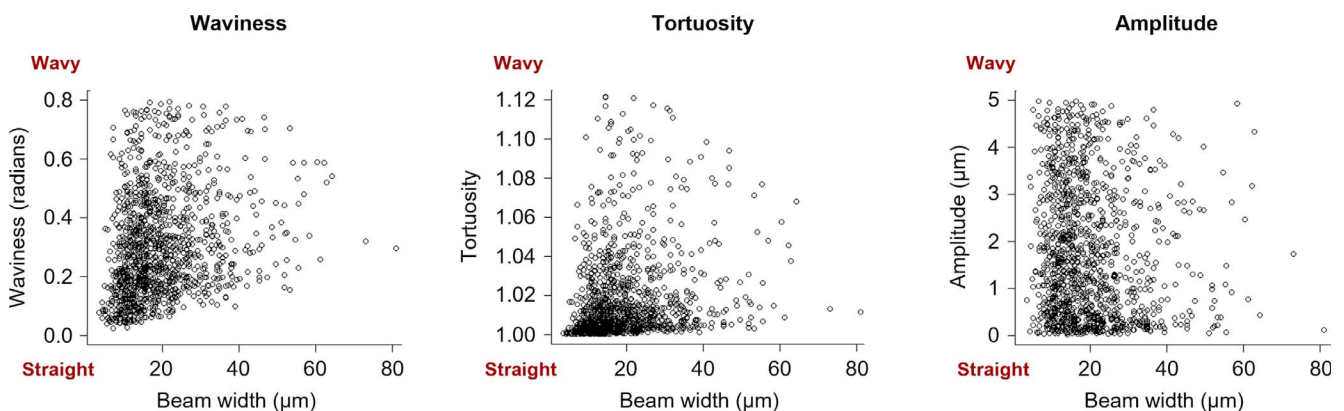

FIGURE 5. Scatterplots of crimp parameters as a function of the beam width when pooling measurements over all the seven eyes. The LC beam width was positively associated with the crimp waviness and tortuosity, and negatively associated with the crimp amplitude (P's < 0.0001).

TABLE. Summary of Results From Statistical Tests (Pooling Measurements Over All the Seven Eyes)

	Waviness			Tortuosity			Amplitude		
Model Type	**Slope**	**AIC**	***P***	**Slope**	**AIC**	***P***	**Slope**	**AIC**	***P***
Linear	0.004	−831	<0.0001	0.0005	−4889	<0.0001	−0.018	4248	<0.0001
Logarithmic	0.018	2293	<0.0001	0.0005	−5057	<0.0001	−0.014	3861	0.0001
Square	**0.003**	**−1426**	**<0.0001**	0.0011	−3026	<0.0001	−0.072	7921	0.0002
Square root	0.004	−1092	<0.0001	**0.0002**	**−6660**	**<0.0001**	**−0.007**	**2057**	**<0.0001**

The crimp morphology parameters (waviness, tortuosity, and amplitude) were transformed according to the model type. The sign of the slope indicated whether the crimp parameter increased (+) or decreased (−) with the LC beam width. The AIC and *P* values were calculated to determine the optimal model. For each crimp parameter, the optimal model was marked in bold, with the lowest AIC and a significant *P* value.

affecting mechanical properties. Several other factors also affect tissue stiffness and response to load, including, but not limited to, fiber type, composition, thickness, alignment and slip conditions, fibril-to-fibril interactions, proteoglycan and elastin content and distribution, and the amount and type of cross-linking between the fibers, and the presence and characteristics of blood vessels within.[23,25,37,40,41] Further research is needed to quantify additional microstructural

characteristics of LC beams to be able to fully characterize the LC response to the loads of IOP and all the factors that contribute to determine its mechanics, and to confirm the predictions made above.

We also found that thick LC beams had smaller crimp amplitude than thin beams. The implications of this finding are not clear, although the effect size was substantially smaller than for tortuosity and waviness. We hypothesize that a small crimp
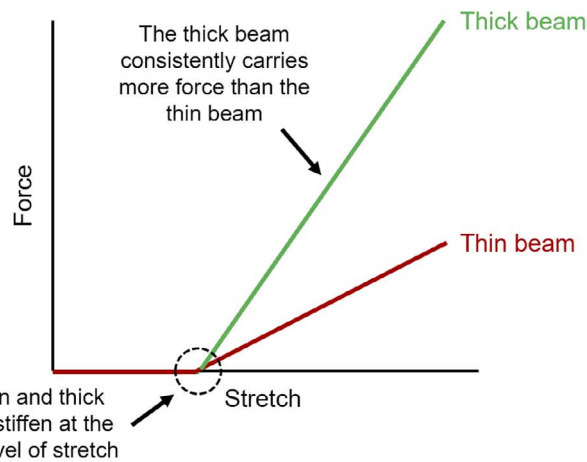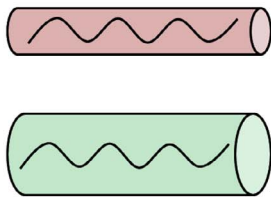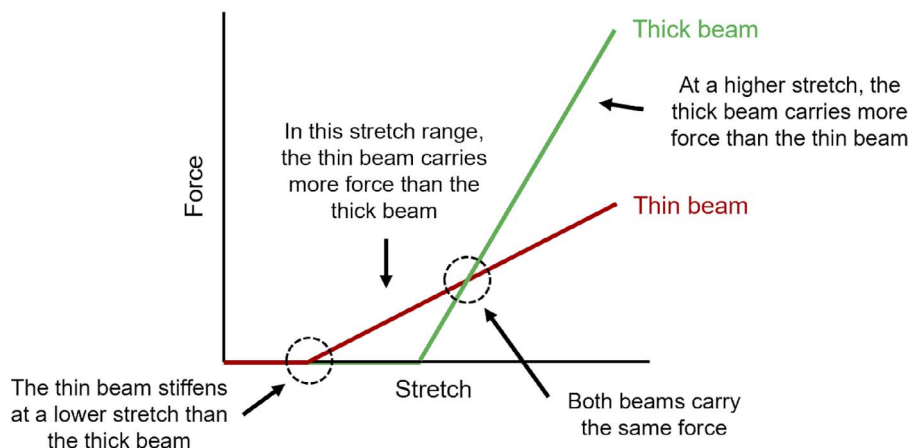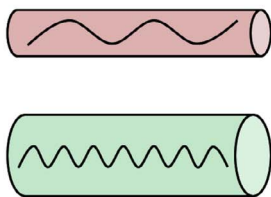

FIGURE 6. Schematic illustration of potential implications of our findings on the relationship between LC beam width and crimp characteristics. We present two cases with different combinations of LC beam width and tortuosity. The first case (*top*) represents the traditional thought that all LC beams have the same mechanical properties, that is, thin and thick beams have the same tortuosity. The second case (*bottom*) represents our experimental findings, in which the thin beam has a lower tortuosity than the thick beam. In the first case, thin and thick beams stiffen at the same level of stretch, with the thick beam consistently carrying more force than the thin beam. Conversely, in the second case, the thin beam stiffens at a lower level of stretch. Hence, for this beam, there is a range of stretches within which the thin beam carries more force than the thick beam. This also results in the existence of a crossover point at which both beams carry the same force. At a higher level of stretch, the thick beam carries more force than the thin beam. For clarity, we do not consider the uncrimping stiffness of collagen fibers in this figure. We refer readers to Supplementary Figure S5, where the force-stretch curve considers the uncrimping stiffness of collagen fibers.

amplitude may facilitate tight collagen fibril packaging and perhaps increased fibril-to-fibril interactions.[42]

Elsewhere, arguments have been made about the connective tissues of the eye remodeling in response to IOP load changes,[43] with age[29,44] and disease.[45] How the collagen of LC beams changes in these conditions remains unknown and should be investigated. Herein we have demonstrated that this can be done using PLM. We are not aware of other studies characterizing LC beam microstructural properties and their relationship with the LC beam width. Several studies, for example in vivo imaging using optical coherence tomography,[18,19,46–49] and ex vivo studies using serial block face imaging,[50] second harmonic generated (SHG) imaging,[5,6,51–54] have quantified LC trabecular beam and pore morphology, including the diameters, but have reported no information on collagen microstructural characteristics, such as the crimp. Accurate measurement of collagen crimp requires high angular and spatial resolutions, otherwise the orientation information will encode both anisotropy and crimp.[55] SHG does have excellent specificity and can image the fibers with micrometer-scale resolution, suitable for crimp studies in some tissues.[56]

In this work, we studied three crimp parameters: waviness, tortuosity, and amplitude. Although these parameters may be related to one another, and not completely independent, our work here and elsewhere[26,28,29,31] shows that each parameter provides a unique perspective on the crimp, and thus they are not redundant. Other parameters can also be used to describe the crimp, such as the period[26,28,31,42] and the maximum deviation angle.[57,58] Future work should look into a better understanding of the relationship between crimp characteristics, perhaps using even higher-resolution imaging techniques that can better identify individual fibers and their orientations, such as polarization-sensitive second harmonic generation microscopy.[59] Future studies should also evaluate the distribution of waviness and tortuosities within the fibers of a beam.

It is important to consider the limitations of our study together with its strengths. The tissues used in this study were ex vivo, fixed in formalin, and cryosectioned, which could introduce artifacts. However, when we looked for effects from tissue fixation and processing, we detected no substantial changes in the architecture of the collagen fibers, including the fiber crimp at the small scale,[27] or tissue distortions at the large scale.[60] The study was conducted on sheep eyes. Sheep eyes, although similar to human eyes because they have a collagenous LC, and because they suffer from IOP-induced glaucomatous-like neuropathy,[61,62] have distinct structural differences from human eyes, such as the ventral groove in the ONH. Also, it remains to be established whether the LC beams are comparable between sheep and humans. It is, therefore, possible that the microstructural crimp characteristics we found in sheep are different from those in humans. Still, it is important to understand sheep as an animal model.[61,62] Future work should include additional animal models, as well as human eyes.

Our measurements of LC beam width were done in coronal sections of the ONH. It is possible that beams were cut partially, resulting a measured beam width smaller than the actual beam diameter. To minimize this risk, we used relatively thick (30-μm) sections of the ONH. Our PLM images mostly show continuous beams, suggesting that we mostly captured whole beams. A similar issue exists in the crimp measures. The fiber orientation information we used to calculate crimp was based on two-dimensional measurements on the plane of the section. We have discussed this issue in detail elsewhere, including potential implications on the measurements.[29,31] Because the beams of the sheep LC are mostly organized in the coronal plane, we posit that this is the most relevant plane for measurement. Future studies,

nevertheless, should quantify crimp parameters in the other planes, potentially using more advanced PLM techniques to obtain three-dimensional (3D) data on crimp.[63] Also, we did not analyze LC beams with energy values under 2% of the energy range. Although our previous studies suggest that this still allowed us to consider the vast majority of beams, even those with pigment or little collagen, it is possible that we may have missed some beams.

A small, non-zero, IOP was necessary to ensure maintaining the shape of the globe, without potential artifactual beam distortions. Hence, the eyes for this study were fixed at 5 mm Hg. Although 5 mm Hg may be high to serve as an ideal undeformed reference state, and below physiologic levels, it can serve as a reference. Elsewhere we compared some collagen crimp characteristics over the whole LC and peripapillary sclera, and found no significant differences between eyes fixed at 0 and 5 mm Hg.[26] Those studies, however, focused on crimp period, not waviness and tortuosity. It seems reasonable to expect that some waviness and tortuosity will vary with the IOP level. Future studies could use the techniques in this work to quantify the dependence of crimp on the IOP level.

It should be noted that the LC beams are not isolated, and instead form part of a complex 3D network, and therefore the biomechanical behavior of a beam is not independent. The trabecular structure of the LC likely plays an important role in its biomechanics.[64,65]

In conclusion, we have presented novel measurements of the microstructural crimp characteristics of the collagen fibers of LC beams. Our measurements show that crimp properties are associated with LC beam width. Because fiber crimp is a main determinant of the biomechanical properties of the beams, our results suggest that thin and thick LC beams have different mechanical properties. This, in turn, suggests that it may not be appropriate to assume that thin LC beams provide less mechanical support to neighboring tissues than thick LC beams. Similarly, our results suggest that it may not be appropriate to infer that LC regions with thin LC beams are necessarily more sensitive to IOP than regions with thick LC beams. Instead, our results support the idea that the collagen fibers of the LC beams vary over the LC and may even remodel or adapt to produce a more uniform structural support than may be inferred solely based on LC beam widths. This study emphasizes the critical need to consider the potential role of microstructure in eye mechanics and physiology, in aging, and in biomechanics-related ocular diseases, such as glaucoma. Nevertheless, further work is needed to obtain direct experimental data on the mechanical properties of the LC tissues and their association with collagen microstructure, including crimp.

References

1. Quigley HA, Addicks EM, Green WR, Maumenee A. Optic nerve damage in human glaucoma: II. The site of injury and susceptibility to damage. *Arch Ophthalmol.* 1981;99:635–649.

2. Sigal IA, Ethier CR. Biomechanics of the optic nerve head. *Exp Eye Res.* 2009;88:799–807.

3. Campbell IC, Coudrillier B, Ethier CR. Biomechanics of the posterior eye: a critical role in health and disease. *J Biomech Eng*. 2014;136:021005.

4. Girard MJ, Dupps WJ, Baskaran M, et al. Translating ocular biomechanics into clinical practice: current state and future prospects. *Curr Eye Res*. 2015;40:1–18.

5. Midgett DE, Pease ME, Jefferys JL, et al. The pressure-induced deformation response of the human lamina cribrosa: analysis of regional variations. *Acta Biomater*. 2017;53:123–139.

6. Sigal IA, Grimm JL, Jan NJ, Reid K, Minckler DS, Brown DJ. Eye-specific IOP-induced displacements and deformations of human lamina cribrosa. *Invest Ophthalmol Vis Sci*. 2014;55:1–15.

7. Quigley HA. Reappraisal of the mechanisms of glaucomatous optic nerve damage. *Eye*. 1987;1:318–322.

8. Exler RE, Guo X, Chan D, et al. Biomechanical insult switches PEA-15 activity to uncouple its anti-apoptotic function and promote erk mediated tissue remodeling. *Exp Cell Res*. 2016; 340:283–294.

9. Rogers RS, Dharsee M, Ackloo S, Sivak JM, Flanagan JG. Proteomics analyses of human optic nerve head astrocytes following biomechanical strain. *Mol Cell Proteomics*. 2012; 11:M111.012302.

10. Hernandez MR. The optic nerve head in glaucoma: role of astrocytes in tissue remodeling. *Prog Retin Eye Res*. 2000;19: 297–321.

11. Balaratnasingam C, Kang MH, Yu P, et al. Comparative quantitative study of astrocytes and capillary distribution in optic nerve laminar regions. *Exp Eye Res*. 2014;121:11–22.

12. Wang R, Seifert P, Jakobs TC. Astrocytes in the optic nerve head of glaucomatous mice display a characteristic reactive phenotype. *Invest Ophthalmol Vis Sci*. 2017;58:924–932.

13. Tehrani S, Davis L, Cepurna WO, et al. Astrocyte structural and molecular response to elevated intraocular pressure occurs rapidly and precedes axonal tubulin rearrangement within the optic nerve head in a rat model. *PLoS One*. 2016; 11:e0167364.

14. Burgoyne CF. A biomechanical paradigm for axonal insult within the optic nerve head in aging and glaucoma. *Exp Eye Res*. 2011;93:120–132.

15. Ishida T, Jonas JB, Ishii M, Shinohara K, Ikegaya Y, Ohno-Matsui K. Peripapillary arterial ring of Zinn-Haller in highly myopic eyes as detected by optical coherence tomography angiography. *Retina*. 2017;37:299–304.

16. Tamm ER, Ethier CR, Dowling JE, et al. Biological aspects of axonal damage in glaucoma: a brief review. *Exp Eye Res*. 2017;157:5–12.

17. Stowell C, Burgoyne CF, Tamm ER, et al. Biomechanical aspects of axonal damage in glaucoma: a brief review. *Exp Eye Res*. 2017;157:13–19.

18. Wang B, Lucy KA, Schuman JS, et al. Decreased lamina cribrosa beam thickness and pore diameter relative to distance from the central retinal vessel trunk. *Invest Ophthalmol Vis Sci*. 2016;57:3088–3092.

19. Wang B, Nevins JE, Nadler Z, et al. In vivo lamina cribrosa micro-architecture in healthy and glaucomatous eyes as assessed by optical coherence tomography. *Invest Ophthalmol Vis Sci*. 2013;54:8270–8274.

20. Quigley HA, Addicks EM. Regional differences in the structure of the lamina cribrosa and their relation to glaucomatous optic nerve damage. *Arch Ophthalmol*. 1981; 99:137–143.

21. Roberts MD, Liang Y, Sigal IA, et al. Correlation between local stress and strain and lamina cribrosa connective tissue volume fraction in normal monkey eyes. *Invest Ophthalmol Vis Sci*. 2010;51:295–307.

22. Bader AN, Pena A-M, van Voskuilen CJ, et al. Fast nonlinear spectral microscopy of in vivo human skin. *Biomed Opt Express*. 2011;2:365–373.

23. Birch HL, Thorpe CT, Rumian AP. Specialisation of extracellular matrix for function in tendons and ligaments. *Muscles Ligaments Tendons J*. 2013;3:12.

24. Franchi M, Raspanti M, Dell'Orbo C, et al. Different crimp patterns in collagen fibrils relate to the subfibrillar arrangement. *Connect Tissue Res*. 2008;49:85–91.

25. Fratzl P. Collagen: structure and mechanics, an introduction. In: Fratzel P, ed. *Collagen*. Boston, MA: Springer; 2008:1–13.

26. Jan NJ, Sigal IA. Collagen fiber recruitment: a microstructural basis for the nonlinear response of the posterior pole of the eye to increases in intraocular pressure. *Acta Biomater*. 2018; 72:295–305.

27. Jan NJ, Grimm JL, Tran H, et al. Polarization microscopy for characterizing fiber orientation of ocular tissues. *Biomed Opt Express*. 2015;6:4705–4718.

28. Jan NJ, Gomez C, Moed S, et al. Microstructural crimp of the lamina cribrosa and peripapillary sclera collagen fibers. *Invest Ophthalmol Vis Sci*. 2017;58:3378–3388.

29. Gogola A, Jan NJ, Brazile BL, et al. Spatial patterns and age-related changes of the collagen crimp in the human cornea and sclera. *Invest Ophthalmol Vis Sci*. 2018;59:2987–2998.

30. Jan NJ, Lathrop K, Sigal IA. Collagen architecture of the posterior pole: high-resolution wide field of view visualization and analysis using polarized light microscopy. *Invest Ophthalmol Vis Sci*. 2017;58:735–744.

31. Jan NJ, Brazile BL, Hu D, et al. Crimp around the globe; patterns of collagen crimp across the corneoscleral shell. *Exp Eye Res*. 2018;172:159–170.

32. Schindelin J, Arganda-Carreras I, Frise E, et al. Fiji: an open-source platform for biological-image analysis. *Nat Methods*. 2012;9:676–682.

33. Yang B, Jan NJ, Brazile B, Voorhees A, Lathrop KL, Sigal IA. Polarized light microscopy for 3-dimensional mapping of collagen fiber architecture in ocular tissues. *J Biophotonics*. 2018;11:e201700356.

34. Gałecki A, Burzykowski T. Linear mixed-effects model. In: Gałecki A, Burzykowski T, eds. *Linear Mixed-Effects Models Using R*. New York, NY: Springer; 2013:245–273.

35. R Development Core Team R. *R: A Language and Environment for Statistical Computing*. Vienna, Austria: R Foundation for Statistical Computing; 2008.

36. Grytz R, Meschke G. Constitutive modeling of crimped collagen fibrils in soft tissues. *J Mech Behav Biomed Mater*. 2009;2:522–533.

37. Holzapfel GA. Biomechanics of soft tissue. In: Lemaitre J, ed. *Handbook of Materials Behavior Models*. Vol. III. Cambridge, MA: Academic Press; 2001:1057–1071.

38. Van Lenthe G, Stauber M, Müller R. Specimen-specific beam models for fast and accurate prediction of human trabecular bone mechanical properties. *Bone*. 2006;39:1182–1189.

39. Klintström E, Smedby Ö, Moreno R, Brismar TB. Trabecular bone structure parameters from 3D image processing of clinical multi-slice and cone-beam computed tomography data. *Skeletal Radiol*. 2014;43:197–204.

40. Ethier CR, Johnson M, Ruberti J. Ocular biomechanics and biotransport. *Annu Rev Biomed Eng*. 2004;6:249–273.

41. Brazile BL, Yang B, Voorhees A, Sigal IA. In-situ measurement of intraocular pressure-induced deformation of the capillaries and collagenous beams of the lamina cribrosa. Paper presented at: World Congress of Biomechanics; July 8–12, 2018; Dublin, Ireland.

42. Liao J, Vesely I. A structural basis for the size-related mechanical properties of mitral valve chordae tendineae. *J Biomech*. 2003;36:1125–1133.

43. Grytz R, Sigal IA, Ruberti JW, Meschke G, Downs JC. Lamina cribrosa thickening in early glaucoma predicted by a microstructure motivated growth and remodeling approach. *Mech Mater*. 2012;44:99–109.

44. Grytz R, Fazio MA, Libertiaux V, et al. Age- and race-related differences in human scleral material properties. *Invest Ophthalmol Vis Sci*. 2014;55:8163–8172.

45. Baldivia S, Levy A, Hegde S, Aper SJ, Merkx M, Grytz R. A novel organ culture model to quantify collagen remodeling in tree shrew sclera. *PLoS One*. 2016;11:e0166644.

46. Ivers KM, Li C, Patel N, et al. Reproducibility of measuring lamina cribrosa pore geometry in human and nonhuman primates with in vivo adaptive optics imaging. *Invest Ophthalmol Vis Sci*. 2011;52:5473–5480.

47. Nadler Z, Wang B, Wollstein G, et al. Automated lamina cribrosa microstructural segmentation in optical coherence tomography scans of healthy and glaucomatous eyes. *Biomed Opt Express*. 2013;4:2596–2608.

48. Wang B, Tran H, Smith MA, et al. In-vivo effects of intraocular and intracranial pressures on the lamina cribrosa microstructure. *PLoS One*. 2017;12:e0188302.

49. Sredar N, Ivers KM, Queener HM, Zouridakis G, Porter J. 3D modeling to characterize lamina cribrosa surface and pore geometries using in vivo images from normal and glaucomatous eyes. *Biomed Opt Express*. 2013;4:1153–1165.

50. Reynaud J, Lockwood H, Gardiner SK, Williams G, Yang H, Burgoyne CF. Lamina cribrosa microarchitecture in monkey early experimental glaucoma: global change. *Invest Ophthalmol Vis Sci*. 2016;57:3451–3469.

51. Albon J, Farrant S, Akhtar S, et al. Connective tissue structure of the tree shrew optic nerve and associated ageing changes. *Invest Ophthalmol Vis Sci*. 2007;48:2134–2144.

52. Brown DJ, Morishige N, Neekhra A, Minckler DS, Jester JV. Application of second harmonic imaging microscopy to assess structural changes in optic nerve head structure ex vivo. *J Biomed Opt*. 2007;12:024029.

53. Ram S, Danford F, Howerton S, Rodriguez J, Geest JV. Three-dimensional segmentation of the ex-vivo anterior lamina cribrosa from second-harmonic imaging microscopy. *IEEE Trans Biomed Eng*. 2018;65:1617–1629.

54. Campbell IC, Coudrillier B, Mensah J, Abel RL, Ethier CR. Automated segmentation of the lamina cribrosa using Frangi's filter: a novel approach for rapid identification of tissue volume fraction and beam orientation in a trabeculated structure in the eye. *J R Soc Interface*. 2015;12:20141009.

55. Pierlot CM, Lee JM, Amini R, Sacks MS, Wells SM. Pregnancy-induced remodeling of collagen architecture and content in the mitral valve. *Ann Biomed Eng*. 2014;42:2058–2071.

56. Hill MR, Duan X, Gibson GA, Watkins S, Robertson AM. A theoretical and non-destructive experimental approach for direct inclusion of measured collagen orientation and recruitment into mechanical models of the artery wall. *J Biomech*. 2012;45:762–771.

57. Grytz R, Meschke G. A computational remodeling approach to predict the physiological architecture of the collagen fibril network in corneo-scleral shells. *Biomech Model Mechanobiol*. 2010;9:225–235.

58. Grytz R, Meschke G, Jonas JB. The collagen fibril architecture in the lamina cribrosa and peripapillary sclera predicted by a computational remodeling approach. *Biomech Model Mechanobiol*. 2011;10:371–382.

59. Vohnsen B, Li JJ, Jan NJ, Sigal IA. Vectorial 3-D polarization second-harmonic imaging of collagen fibril organization in the lamina cribrosa. Paper presented at: 18th European Light Microscopy Initiative Meeting; June 5–8, 2018; Dublin, Ireland.

60. Tran H, Jan NJ, Hu D, et al. Formalin fixation and cryosectioning cause only minimal changes in shape or size of ocular tissues. *Sci Rep*. 2017;7:12065.

61. Candia OA, Gerometta RM, Danias J. Tissue plasminogen activator reduces the elevated intraocular pressure induced by prednisolone in sheep. *Exp Eye Res*. 2014;128:114–116.

62. Gerometta R, Spiga MG, Borras T, Candia OA. Treatment of sheep steroid–induced ocular hypertension with a glucocorticoid-inducible MMP1 gene therapy virus. *Invest Ophthalmol Vis Sci*. 2010;51:3042–3048.

63. Yang B, Jan NJ, Brazile B, Voorhees A, Lathrop KL, Sigal IA. Polarized light microscopy for 3D mapping of collagen fiber architecture in ocular tissues. *J Biophotonics*. 2018;11: e201700356.

64. Voorhees A, Jan NJ, Sigal IA. Effects of collagen microstructure and material properties on the deformation of the neural tissues of the lamina cribrosa. *Acta Biomater*. 2017;58:278–290.

65. Voorhees AP, Jan NJ, Austin ME, et al. Lamina cribrosa pore shape and size as predictors of neural tissue mechanical insult. *Invest Ophthalmol Vis Sci*. 2017;58:5336–5346.